Electronic Supplementary Material (ESI) for Journal of Materials Chemistry A.

A $CaCO_3$/nanocellulose-based bioinspired nacre-like material

Masoud Farhadi-Khouzani[a], Christina Schütz[b,†], Grażyna M. Durak[a], Jordina Fornell[c], Jordi Sort[d], Germán Salazar-Alvarez[b], Lennart Bergström[b], Denis Gebauer[a,*]

a) Department of Chemistry, Physical Chemistry, University of Konstanz, Universitätsstr. 10, Box 714, D-78457 Konstanz, Germany).

b) Department of Materials and Environmental Chemistry, Stockholm University, SE-10691 Stockholm, Sweden; Wallenberg Wood Science Center, Teknikringen 56, SE-100 44 Stockholm, Sweden

c) Departament de Física, Universitat Autonoma de Barcelona, E-08193 Bellaterra, Spain

d)Institucio Catalana de Recerca i Estudis Avancats (ICREA), Pg. Lluís Companys 23, E-08010 Barcelona, Spain and Departament de Física, Universitat Autonoma de Barcelona, E-08193 Bellaterra, Spain

† Current address: Department of Chemical Engineering, KU Leuven, Campus Kulak Kortrijk, 8500 Kortrijk, Belgium

S1. Experimental

S1.1. Preparation and functionalization of nanocellulose samples

Cellulose nanofibers (NC-OH)

The nanofibrillated cellulose was prepared from never dried softwood sulphite pulp (Nordic Paper, Seffle AB, Säffle, Sweden; the degree of polymerization of cellulose was 1200, the cellulose content was approximately 86 %, the rest is mainly hemicelluloses and lignin) using enzymatic procedure developed by Henriksson et al.[1] Subsequently, pre-treated fibres were disintegrated by a homogenization process using a microfluidizer M-110EH (Microfluidics Inc., USA) for three passes through bigger chambers (diameter of 400 and 200 μm), and five passes through small chambers (diameter of 200 and 100 μm). A suspension of approximately 2 wt% of NC-OH was obtained. The surface charge of averaged three measurements resulted in 9.9 μmol/g determined by polyelectrolyte titration with a 0.001 N polydiallyl dimethyl ammonium chloride solution.

Bacterial cellulose nanocrystals (BNC-SO_3H)

Coconut gel cubes (ca. 1x1x1 cm^3, Chaokoh, Thailand) were washed three times with 2 dm^3 of deionized water and stirred in 2 dm^3 of a 0.1M sodium hydroxide solution for 48 hours and then

washed with deionized water until the pH stabilized at around 7. 100 g of bacterial cellulose cubes were hydrolyzed by approximately 40% sulfuric acid at 80°C for 4 h. The reaction was quenched by dilution with 10-fold amount of deionized water and the resulting suspension was washed two times by centrifugation with deionized water. The precipitant was collected and dialyzed against deionized water using Sigma Aldrich dialysis membranes with a molecular weight cut off of ~14000 for 5–7 days. After the dialysis the suspension was sonicated for 10 min with an output of 70% (Vibra-Cell VC 750, Sonics, USA), using a 13 mm wide titanium probe, followed by centrifugation for 60 min at 4020 RCF to remove the titanium nanoparticles introduced. The surface charge of the systems was determined by polyelectrolyte titration using a Stabino Particle Charge Mapping system (Microtrac Europe GmbH, Germany). The dispersions were dispersed in MilliQ water and then titrated with a 0.001 N polydiallyl dimethyl ammonium chloride solution. Every titration was repeated at least 3 times and the average value resulted in 0.03 mmol/g.

Cellulose nanocrystals (NC-COOH)

The cellulose nanocrystal (NC-COOH) were prepared by hydrochloric acid hydrolysis of the TEMPO-oxidized cellulose nanofibers (CNF-COOH) according to Salajková et al.[2] 100 g of CNF-COOH gel (1 g dry weight of cellulose) was dispersed in 316 mL deionized water and stirred over night. Hydrochloric acid was added to reach a final concentration of 2.5M and the mixture was heated to 100°C for 6 h. The reaction was quenched by dilution with 5-fold amount of deionized water. The resulting suspension was washed by centrifugation twice with deionized water. The precipitant was collected and dialyzed against deionized water using Sigma Aldrich dialysis membranes with a molecular weight cut off of ~14000 for 5 days. After the dialysis the suspension was sonicated for 10 min with an output of 70% (Vibra-Cell VC 750, Sonics, USA), using a 13 mm wide titanium probe. The suspension was centrifuged (60 min at 4020 RCF) in order to remove the introduced titanium particles and remaining aggregates. The surface charge of the systems was determined by polyelectrolyte titration using a Stabino Particle Charge Mapping system (Microtrac Europe GmbH, Germany). The dispersions were dispersed in MilliQ water, adjusted to pH 10 and then titrated with a 0.001 N polydiallyl dimethyl ammonium chloride solution. Every titration was repeated at least 3 times and the average value resulted in 0.4 mmol/g.

S1-2 Coating of NCs on the surface

Deposition of NCs on the silicon wafer substrate was performed using the drop casting method. Nanocellulose dispersions used for the experiments were shaken and sonicated for 15 min before usage. Silicon wafers were selected as substrates suitable for deposition of the layered composites. The substrates were washed with four different solvents: toluene, acetone, iso-propanol and ethanol in the order from the lowest to the highest polarity. Si wafers were immersed in each solvent, sonicated for 5 min and then dried. Next, 100 µl of the desired nanocellulose dispersion was aspirated with a pipette and deposited on the surface of the Si wafer. Si wafers were then dried in the vacuum oven at 40 °C and 50% relative humidity for ca. 2 h or until all solvent evaporated.

S1-3 Stability of various nanocellulose films under mineralization conditions

As the gas mineralization assay is based on diffusion of ammonia and carbon dioxide released during decomposition of ammonium carbonate, testing the stability of NC films in calcium chloride solution before and after addition of ammonia is crucial to ensure the attachment of the initial layer to the substrate before a free-standing layered composite can be obtained. Therefore, the stability of different nanocellulose films prepared by drop-casting method was examined by immersing the films in 10 ml of 10 mM calcium chloride solution (pH 7.25). This was followed by testing the film stability under basic conditions by adding 50 µl of concentrated ammonia to the calcium chloride solution. The treatments of the films were performed for one day. After each step, the films were analyzed with transmission FT-IR. Three different types of nanocellulose films were chosen for this test; cellulose nanocrystals functionalized with carboxyl groups (NC-COOH), bacterial nanocellulose functionalized with sulfonate groups (BNC-SO_3H) and cellulose nanofibrils carrying OH functions (NC-OH). The results suggest that all of the films are still stable after treatment with calcium chloride and there are no significant changes in terms of band intensities in the FT-IR spectra collected in transmission mode (Fig. S2). The only exception was a shift in the position of the carboxyl band (1718 cm^{-1}) towards lower wavenumbers in the NC functionalized with carboxyl groups, which may be related to chelation of calcium by carboxyl groups.

Addition of concentrated ammonia and treatment of the films under basic conditions did not affect the NC-OH and NC-COOH film stability, however, BNC-SO_3H films completely detached from the substrate. FT-IR analysis of the BNC-SO_3H film deposited on a Si wafer substrate shows weak bands where the residual BNC was detected after treatment with ammonia indicating that majority of the film was washed away (Fig. S-2(c)). Hence we used NC-OH and NC-COOH as the organic components of the multilayered films for the preparation of the nacre mimics.

S1-4 Gas diffusion mineralization assay

We used the gas diffusion method for the mineralization of the nanocellulose films with calcium carbonate. To that end as well as for investigation of wettability by the PILP precursors, we prepared 10 ml of four solutions in 20 ml vials in which the nanocellulose films were placed face-up at the bottom. Further details and composition of the solutions are summarized in table 1. All of the vials were covered with parafilm and a single pinhole was pierced in the parafilms for diffusion of the gas. Ca. 10 g of ammonium carbonate was placed at the bottom of a 20 ml vial in the lower compartment of a desiccator. The vials with the nanocellulose films immersed in different solutions were placed on the ceramic plate in the upper desiccator compartment. The dissector was then sealed with a round-glass rim and incubated at 25 ± 1 ºC. Dramatic deviation from this temperature will influence the decomposition rate of ammonium carbonate and consequently diffusion rate of ammonia and hence have a significant effect on the mineralization.

S1-5 Further mineralizations

After the first mineralization, two more layers were coated on top of the mineralized layer. Note that homogeneity of mineralized film is essential for achieving smooth layers. Therefore, it is important to choose the film with right thickness as well as appropriate mineralization condition. The second further layers are dependent on the first mineralized layer. In the absence of Mg^{+2}, the first layer is NC-OH which was mineralized and then, NC-COOH as a second layer and another NC-OH layer as the third layer was coated on top of mineralized NC-OH. Then, the same process was performed for subsequent mineralization of the prepared films.

S2. Analyses

S2-1 SEM analysis

The SEM images of layered nacre mimic structures were acquired with the FESEM Auriga Crossbeam (Carl Zeiss Microscopy GmbH, Oberkochen, Germany) equipped with a Silicone Drift Detector Oxford X-Max 20mm² (Oxford Instruments plc, Abingdon, England). Samples were embedded in Epo Fix resin it (including resin and hardener) prior to cross-section SEM imaging. For each sample, ca. 10 g resin and 2 g hardener were mixed for ca. 2 min and then the mixture was aspirated with a pipette and deposited on top of the sample. After 12 h polymerization time, the sample was cut in a half with a razor blade and fixed on a stub with carbon tape. X-ray mapping was processed with the INCA 4.15 software (Oxford Instruments plc, Abingdon, England).

The microscopy analyses of the effects of different kinetic reaction parameters on the nanocellulose films were mostly performed using a table-top TM3000 Hitachi microscope.

S2-2 FT-IR analysis

Fourier transform ATR (Attenuated Total Reflection) infrared (ATR/FT-IR) spectra and transmission FT-IR spectra were recorded with a PerkinElmer spectrum 100 spectrometer equipped with a diamond crystal based ATR accessory. The infrared spectra were recorded in the spectral range of 4500-650 cm^{-1} with a resolution of 0.5 cm^{-1}.

S2-3 Thermogravimetric analysis (TGA)

TGA measurements were performed using a simultaneous thermal analyzer instrument, NETZSCH STA 449 F3 *Jupiter*® under oxygen atmosphere with a heating rate of 10 ℃/min. According to the manufacturer's specifications, the weight accuracy of this machine is 0.1 µg over the entire weighing range with a drift smaller than 5 µg/h. The calibrations were accomplished utilizing the calibration kit from the accessories of the instrument whereas the actual crucible of the measurements was used. Furthermore, the TGA traces were corrected by curves obtained by placing the empty crucible in the sample holder and heating in the same manner as during the actual measurements. These corrections were performed in order to exclude baseline artifacts. The TGA measurements of the nacre mimics were performed by placing ca. 10

mg of the dried and neat sample in the crucible and heating the sample in the range of 25-900°C (reference and correction as outlined above).

S2-4 Microtome sectioning and TEM analysis

Samples embedded in Epofix resin were cut into thin sections at room temperature using a Leica Microtome UC6 equipped with a diamond knife. The transmission electron microscopy (TEM) measurements were performed using an In-column OMEGA filter microscope (Zeiss Libra 120) at 120 kV, which has a point resolution of 0.34 nm. In order to inhibit samples to be burned due to irradiation, several tests were performed to find the optimum illumination angle, the optimum size of objective aperture was found to be 130-160 µm. However, due to intrinsic characteristics of nanocellulose and $CaCO_3$ thin sections, which are not stable under illumination of electron beam, most of analysed samples showed partial deterioration. The thin cut samples were placed on 400 mesh copper grids coated with carbon.

S2-5 Confocal Microscopy

Samples were incubated in 10 µg/ml Calcofluor White (CW, Sigma-Aldrich) and 50% ethanol for 6 h. The unbound dye was removed by washing the sample 3 times with 10 ml 50% ethanol followed by an overnight incubation in 50% ethanol to remove any residual dye. CW targets β 1,3- and β 1,4- linkages and was used for labelling the nanocellulose (NC-COOH and NC-OH) prior to Confocal Laser Scanning Microscopy (CLSM). Mineral component of the composite was imaged with reflected light. CLSM images were acquired with a Zeiss LSM 880 microscope using λ=405 nm excitation with a diode laser for both CW and reflectance. CW emission was collected between λ=436-493 nm. Reflected light was collected using a MBS T80/R20filter set and the reflection mode switched on, with the band width between λ=401-411 nm. Images for the Z-stacks were collected at 1 µm intervals and assembled into a 3D representation using the ZEN Software (Carl Zeiss).

S2-6 Mechanical properties analyses

The indentations were carried out using a nanoindenter XP from MTS, in the load control mode, maximum applied force of 5 mN, and using a Berkovich pyramidal-shaped tip. The hardness and “reduced Young’s modulus” were calculated using the method of Oliver and Pharr. The indentation energies were calculated from the areas enclosed between the unloading segment and

the displacement axis (elastic energy, U_{el}) and between the loading segments and displacement axis (total energy, which is: $U_{el} + U_{pl}$, where U_{pl} is the plastic energy). Note that the "reduced Young's modulus" takes into account the elastic displacement that occurs in both, the sample and the indenter:

$$\frac{1}{E_r} = \frac{1 - v_m^2}{E_m} + \frac{1 - v_i^2}{E_i} \quad (1)$$

where subindexes *m* and *i* refer to the material and the indenter, respectively, and ν is the Poisson's ratio. For diamond, $\nu_i = 0.07$ and $E_i = 1140$ GPa. In practice, the values of E_r and E_m are close to each other. Since we do not know the exact value of the Poisson's ratio for the samples, it is better to report the values of E_r, rather than E_m.

Since the samples were relatively thin, a maximum load of 5 mN was used for all measurements. In this way, one can ensure that the maximum penetration during nanoindentation is below $1/10^{th}$ the overall thickness of the films. This is considered as a rule of thumb to avoid the influence from the substrate on the obtained results. For statistical purposes, on average, approximately 25 indentations were performed per sample.

The nacre sample (*Haliotis laevigata)* was cleaved and the inner part which was not polished was chosen for nanoindentation measurements. The sample was then indented on top, after polishing it up to 4000 grit SiC abrasive paper using the same conditions as for the nacre-like material ($P_{max} = 5$ mN). In this case, larger Hardness and Young's modulus values were obtained in agreement with some reports in the literature.[3] However, other studies reported much lower Young's modulus and Hardness values than the ones observed in this report.[4] This observation is due to differences in species, the origin, as well as the specific conditions under which the nanoindentation analysis was performed.[5]

S3 Discussions

S3-1 Analyses of wettability of PILP precursors

S3-1-1 Wettability of nanocellulose films in the absence of Mg^{+2}

In order to be able to construct a structure inspired by nacre, which consists of layers of minerals separated by layers of organics, it is crucial to have films of nanocellulose, which have distinct wettabilities for calcium carbonate PILPs in difference conditions. In fact, Mg^{+2} can tune the wettability of calcium carbonate precursors depending on the functional groups of respective fiber.[6] In order to characterize the wettability of NC-OH and NC-COOH films, mineralization experiments were performed in the presence and absence of Mg^{2+} and mineralized films after each mineralization were analyzed. Fig. S3 shows the SEM images of NC-OH and NC-COOH films before and after mineralization. As it can be seen, after mineralization, $CaCO_3$ with different morphologies exists in both samples. Comparing the morphology of NC-OH fibers before mineralization (Fig. S3(a)) and after mineralization (Fig. S3(e)), it seems that the nanocellulose fibers after minerlization are more smooth, due to the mineralization of the fibers. This is consistent with the BSE-SEM image of the sample showing different contrast of the layers where unmineralized NC-COOH layers are darker (Fig. S10). While micron-sized $CaCO_3$ particles exist also on NC-COOH film, the way that these particles precipitate on the film is similar to interaction of oil on a hydrophilic surface, where the oil droplets tend to aggregate to form larger and more bulky spherical particles and avoid contact with the surface. Therefore, it can be concluded that NC-COOH fibers cannot be wetted with $CaCO_3$ precursors and cannot be mineralized in the absence of Mg^{2+}. The efforts for elemental mappings of mineralized thin films caused the sample to be burned, which made it impossible to unambiguously characterize the composition of the films (data not shown). Changing the kinetics of the mineralization opens up the possibility to investigate the wettability preference of the different types of nanocellulose in more detail. SEM images of samples, which were mineralized for a shorter time, also confirm the low tendency of NC-COOH to $CaCO_3$ precursors in the absence of Mg^{2+} (Fig. S4). Even after 12h of mineralization without Mg^{+2}, $CaCO_3$ covers the entire NC-OH surface and there is barely any uncovered area. However, the back-scattered electron SEM image shows mostly a dark contrast coming from soft materials meaning that NC-COOH film after mineralization hardly contains any $CaCO_3$. To support the obtained results with spectroscopic techniques, ATR/FT-IR

analysis was performed. FT-IR analyses of mineralized samples in different time intervals are summarized in Fig. S5. Although it is not possible to draw any conclusion about interactions between the nanocellulose fibers and $CaCO_3$ based on the FT-IR spectra, due to the limited penetration depth of the IR beam, the coverage of fibers by calcium carbonate becomes evident. It can be seen that the ATR spectra of mineralized NC-OH at all times do not show any organic bands indicating that the fibers are completely covered with $CaCO_3$, while ATR spectra of NC-COOH films at the same time, exhibit strong organic vibrations at around 1050 cm^{-1}. This band comes from the nanocellulose fibers, which are not entirely covered with $CaCO_3$.

S3-1-2 Wettability of nanocellulose films in the presence of Mg^{+2}

In order to elucidate the wettability of nanocellulose films in the presence of Mg^{2+}, mineralizations were performed under different conditions, and again the mineralized films were analyzed. Fig. S14 shows the SEM images of mineralized NC-OH and NC-COOH films in the presence of Mg^{2+}. Mg^{2+} can stabilize amorphous calcium carbonate (ACC) and therefore, the obtained films are in fact nanocellulos-ACC hybrids. The obtained hybrid films, however, show a different mineralization pattern than without magnesium. As it can be seen from Fig. S14, the mineralized NC-COOH film shows a complete coverage with ACC, while SEM images of NC-OH films after mineralization show plenty of fibers, which are still naked especially in the zoomed-in view (Fig. S14 (d)). However, the difference in wettability of NC-OH and NC-COOH in the presence of magnesium is even more pronounced for mineralizations performed for three days. As it can be seen from Fig.S15(a), the mineralized NC-OH film shows huge cracks and even some parts are peeled off from the surface. The reason might be due to uncovered fibers after three days, which makes the film detached. The elemental mapping by EDX (Fig. S15 (e)) on one of these cracks shows that there is only a trace of residual carbon on the silicon wafer, meaning that most of organics are detached. This is not the case, though, for NC-COOH films after mineralization under the same conditions. As it can be seen from Fig. S15 (b), the mineralized film keeps its integrity even after mineralization for three days indicating the covered fibers with $CaCO_3$ are stabilizing the film.

S3-2 Effect of thickness on mineralization of $CaCO_3$ into nanocellulose films

The effect of thickness of the obtained films before mineralization on the homogeneity of obtained $CaCO_3$ films was investigated. Fig. S6 shows focused ion beam (FIB) cutting analyses

of NC-OH thin films, which were prepared from NC-OH dispersions with different concentrations. The results show consistent correlations between the concentration of the dispersions and the obtained film thickness, which means that for instance by decreasing the concentration by a factor two, the thickness is also decreased by a factor two. The dispersions of NC-OH in water are colloidally stable for a few hours in the concentration range of ca. 0.03-0.3 wt. % due to lack of electrostatic interactions between the nanocellulose fibers. Therefore, before drop casting of the nanocellulose dispersions, it was shacked and sonicated for ca. 15 min. However, the NC-COOH is colloidally stable for longer times in almost the whole range of concentrations. As the homogeneity of the obtained films via drop casting correlates with stability of colloidal dispersions, the control over the colloidal dispersions enabled us to obtain smooth films.

The effects of the film thickness of unmineralized nanocellulose films for the outcome of mineralization were also investigated. For this purpose, nanocellulose films with different thickness were prepared, and were mineralized at two conditions (with and without Mg^{+2}). Afterwards, the mineralized films were analyzed in order to illustrate the influence of the thickness of unmineralized thin films on the mineralization outcome. Fig. S7 shows the morphology of mineralized NC-OH films with thicknesses before mineralization of ca. 2.5 µm (from 0.29 wt %), and ca. 410 nm (from 0.055 wt %). The mineralized NC-OH film with lower thickness shows a nearly homogenous coverage of $CaCO_3$ all over the film, while only disintegrated spherical particles can be seen on the thicker film. This observation might be explained by an infiltration problem of liquid precursors due to a different packing of fibers in thicker films. In this case, there is no room or time for infiltration of $CaCO_3$ into the whole film, and only the surface of the films was wetted with $CaCO_3$. Fig. S8 shows a matrix of different conditions, which are required to obtain homogenous mineralized film in order to be able to continue coatings and mineralizations on top of mineralized layers. Without a good quality film and appropriate mineralization conditions, the preparation of homogenous NC-OH films and a layered nacre mimic is not feasible.

S3-3 Mineralization of NC-COOH in presence of Mg^{2+}

While the thickness of the mineralized NC-COOH film can be controlled (Fig. S16), in a similar manner as for the NC-OH films (see main manuscript), the generation of an ACC-based multi-

layered nacre mimic was not feasible in this case, due to appearance of cracks in the composite already after the second mineralization and then further on, leading to a peeling off of the layers away from the substrate (Fig. S17). This may be due to water loss from the ACC and nanocellulose upon drying of the films, which may result in shrinkage of the films, or detaching of the NC-COOH inter-layer when exposing it to the basic mineralization solution. However, the change in wettability demonstrates that the localization of mineralization via PILP can be controlled by the addition of Mg^{2+} for distinct surface functionalizations also in the case of nanocellulose, which is an invaluable tool for controlling mineralization sites.

S4 Figures

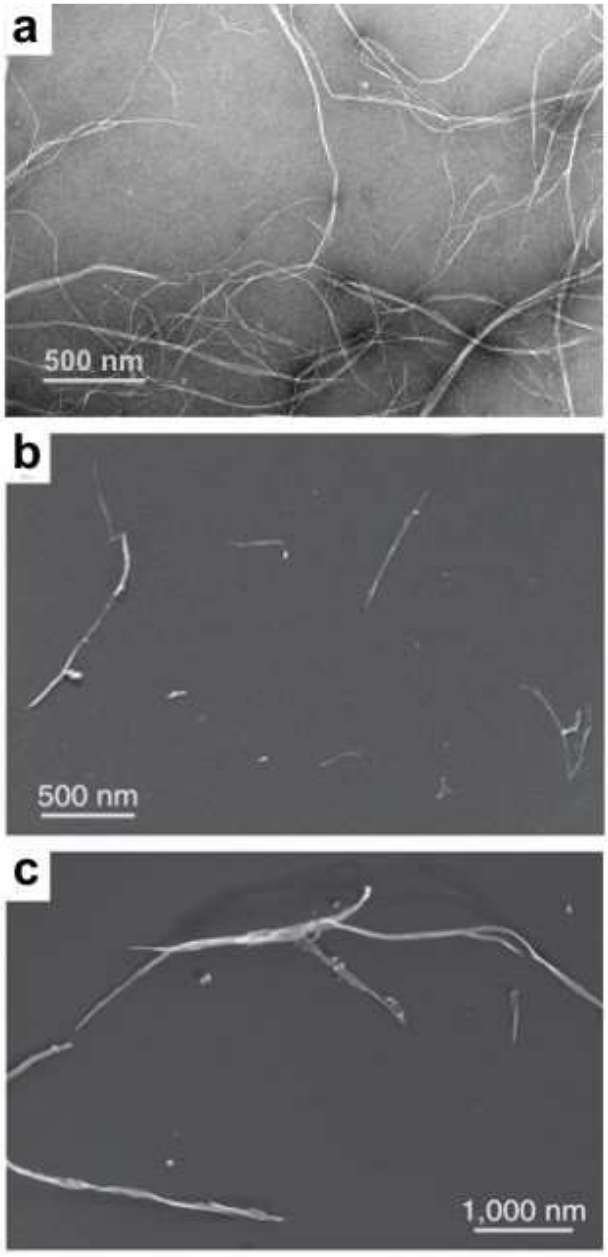

Figure S1: TEM micrographs of (a) NC-OH; (b) NC-COOH; (c) BNC-SO_3H. Note that (b, c) are taken from Usov et al.[7] where the same types of NCs were investigated. The width and length of the NC-OH fibers are ca. 50-100 nm and 2-10 µm, respectively. The NC-COOH crystals are ~3-30 nm in length, and ~0.1-1 µm in width. The width and length of BNC-SO_3H are ~10-50 nm and 1-5 µm, respectively.

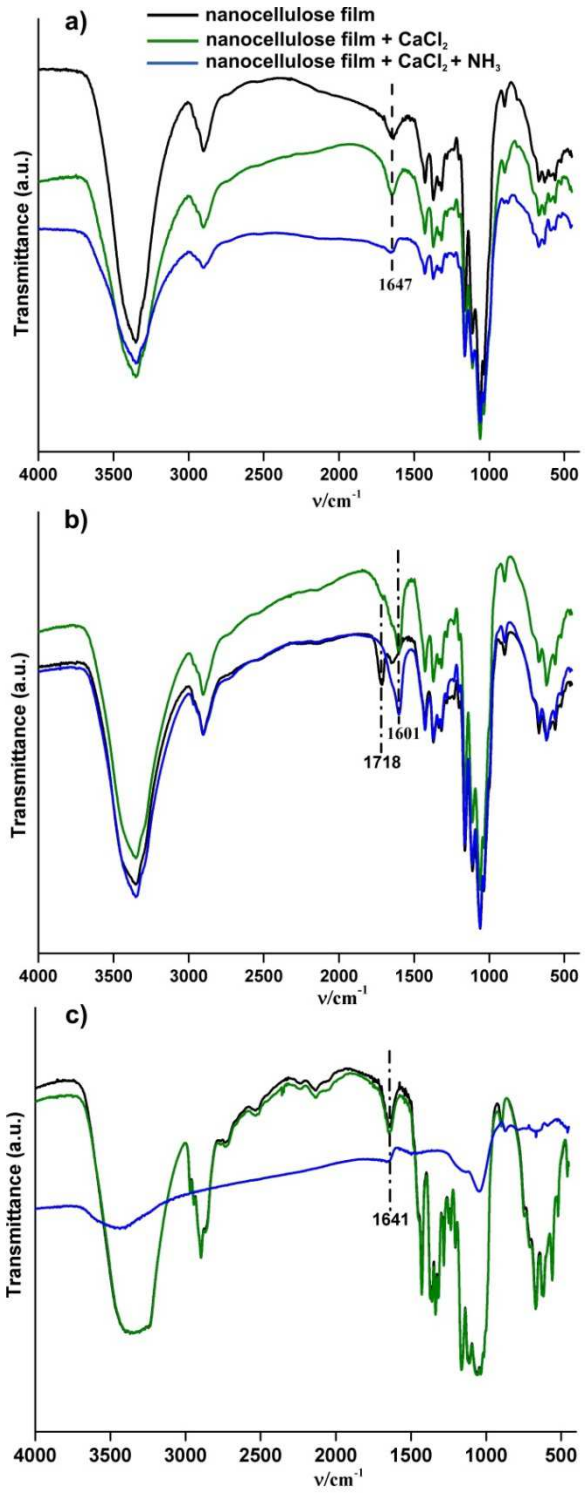

Fig. S2: Transmission FT-IR spectra of a) NC-OH, b) NC-COOH, and c) BNC-SO_3H films before and after treatment with calcium chloride and ammonia as indicated.

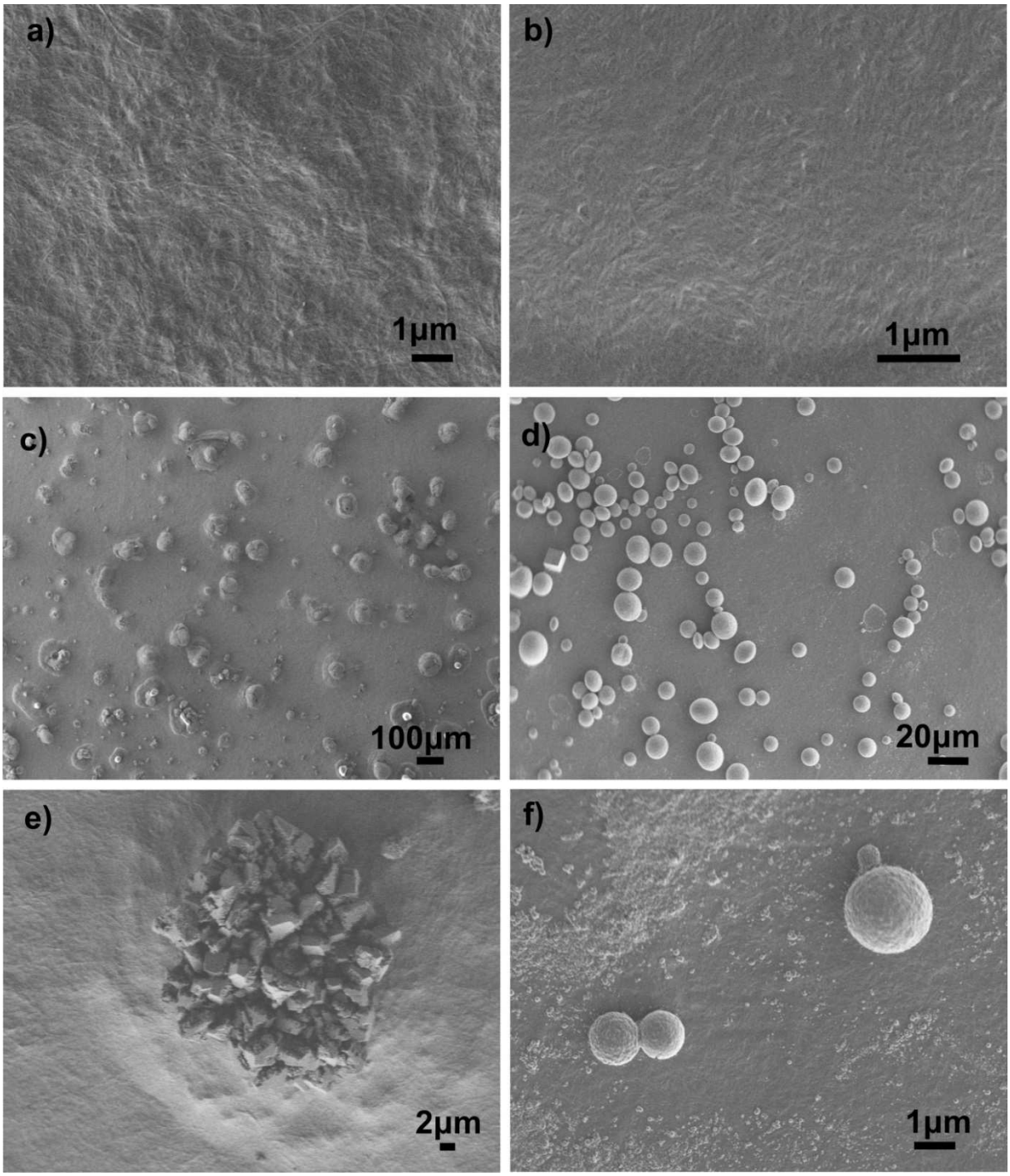

Fig. S3: Comparison of different mineralizations of films in the absence of Mg^{2+}; NC-OH films (a) unmineralized (c, e) mineralized. NC-COOH films (b) unmineralized (d, f) mineralized. Mineralization condition: $CaCl_2$: 10 mM and 100 µg/ml pAsp for 3 days.

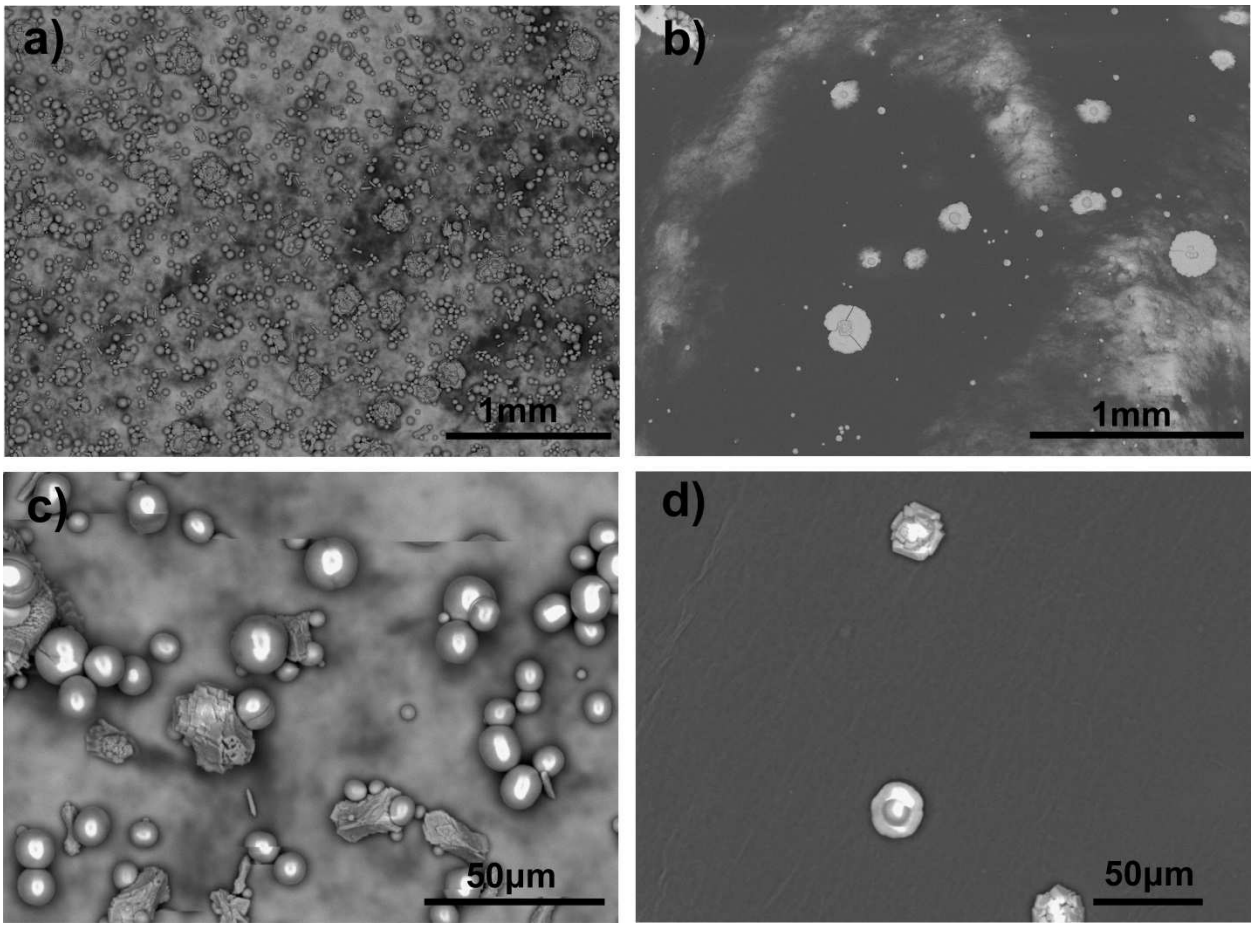

Fig. S4: comparison of mineralization of NC-OH (a, c) and NC-COOH (b,d) films in the absence of Mg^{+2}. Conditions: 5 mM of $CaCl_2$, 100 µg/ml of pAsp, and for 12 h.

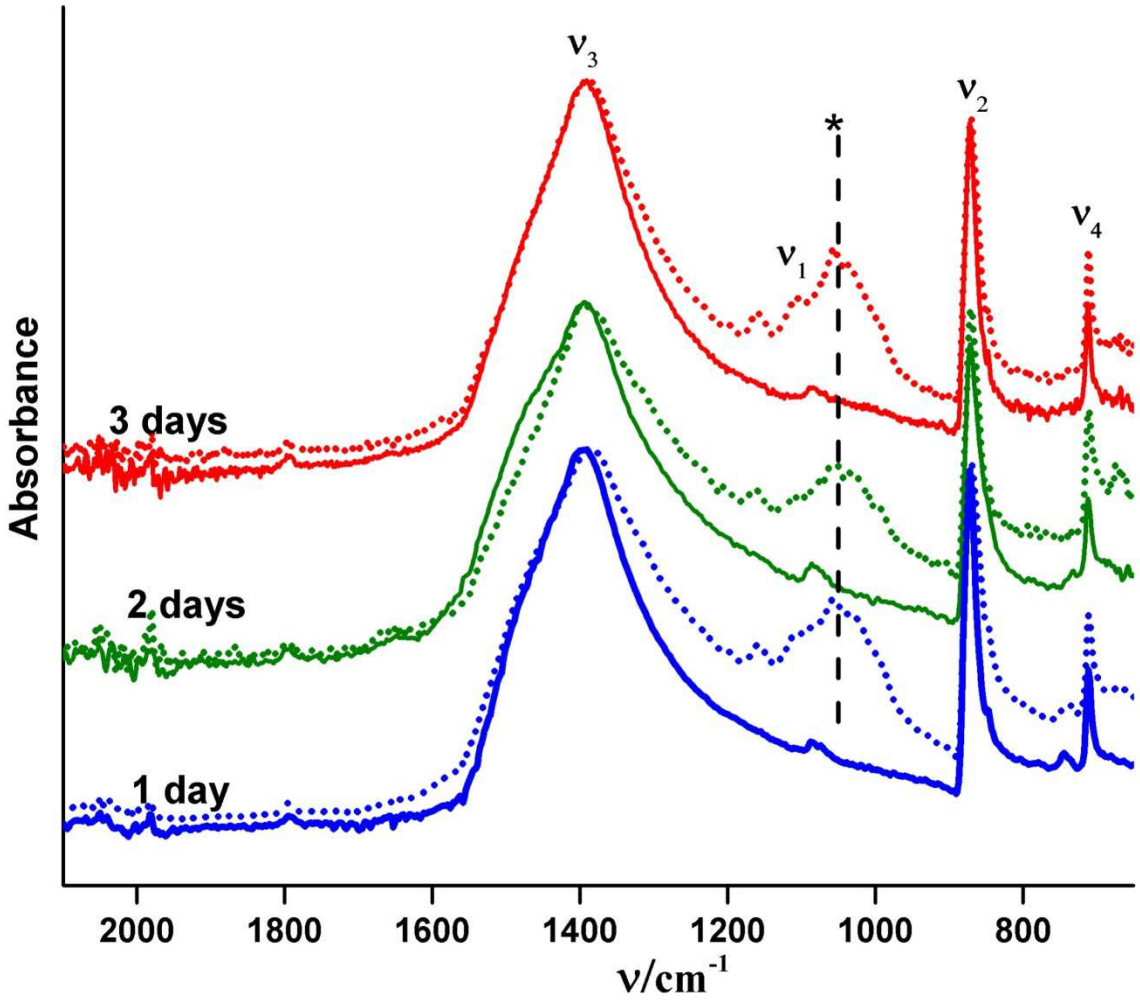

Fig. S5: ATR/FT-IR spectra of mineralized NC-OH films (solid spectra) and NC-COOH films (dashed spectra), which were mineralized for 1, 2, and 3 days in the presence of 10 mM $CaCl_2$ and 100 µg/ml poly(aspartic acid) as indicated. The asterisk labels vibrations from the organics.

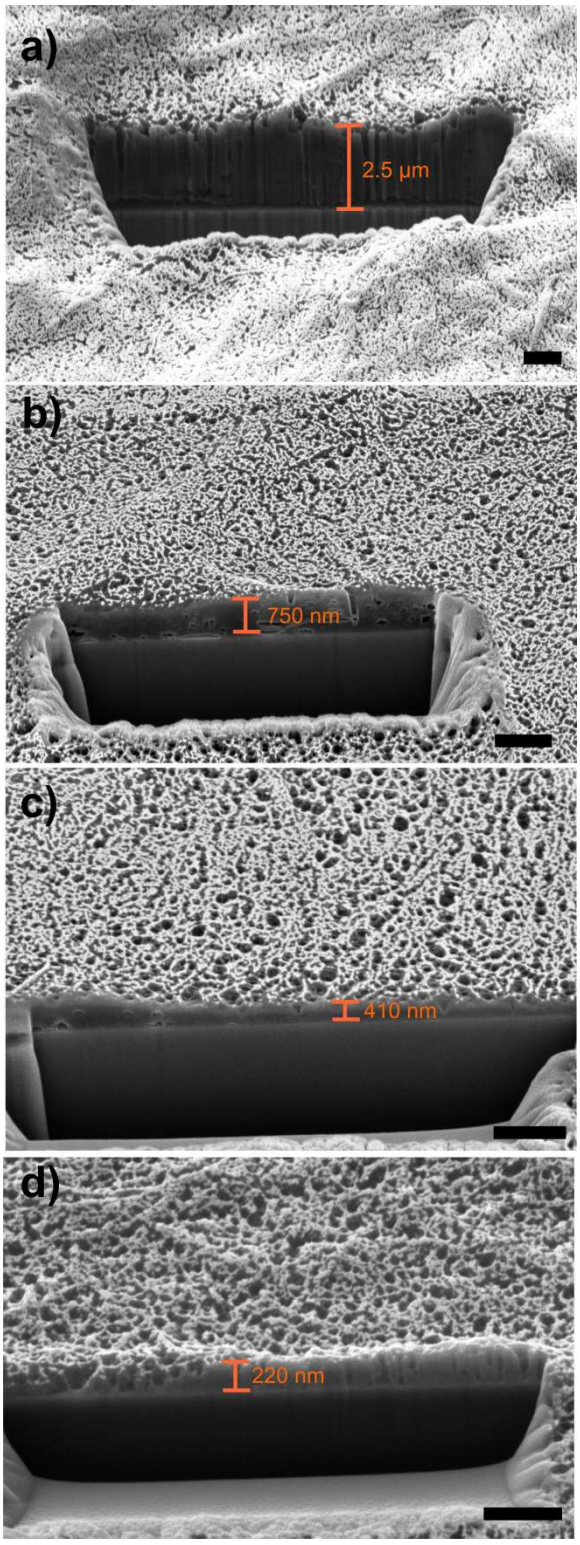

Fig. S6: FIB cutting of NC-OH single layer films prepared from (a) 0.29 wt %, (b) 0.11 wt %, (c) 0.055 wt %, (d) 0.029 wt % dispersions (all scale bars 1 µm). The values given in the images represent an average of the thickness measured at three parts of the FIB cut (left, middle, right), and were placed at a part of the cut where the thickness agreed with this average.

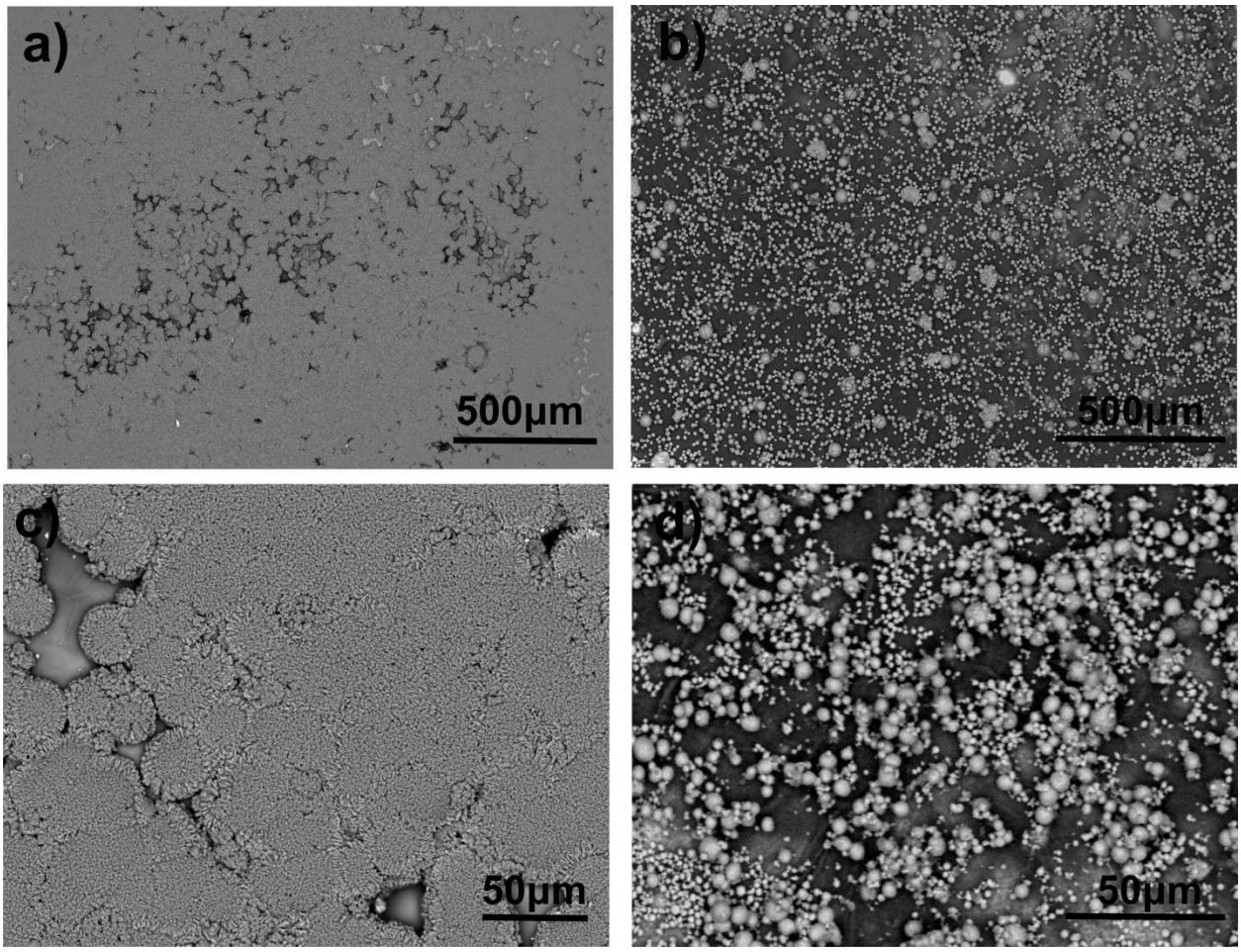

Fig. S7: SEM images of mineralized NC-OH films prepared from films with a thickness of (a, c) 750 nm and (b, d) 2.5µm. Mineralization conditions: 5 mM $CaCl_2$ and 100 µg/ml pAsp for 3 days.

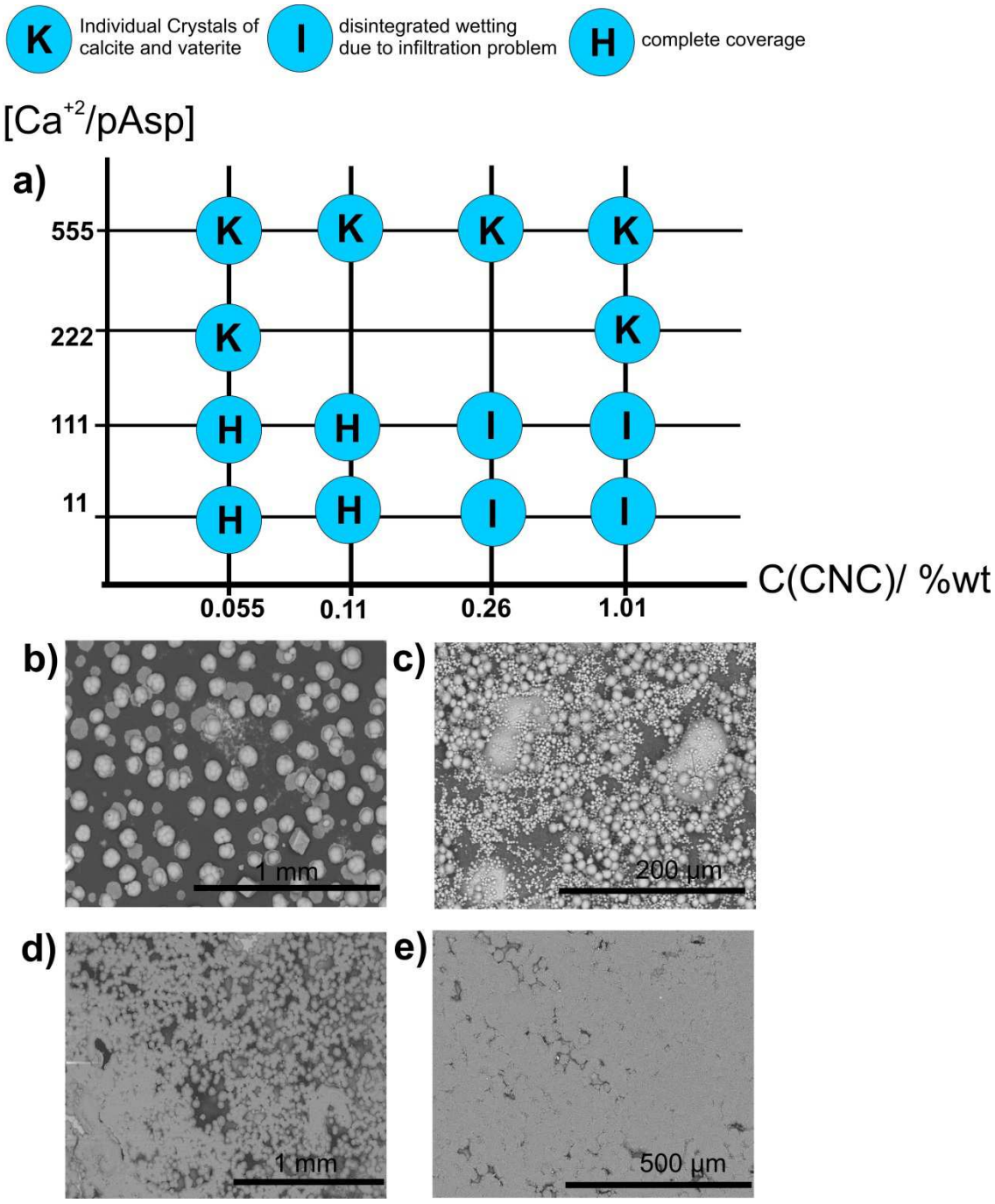

Fig. S8: a) The matrix summarizes the influence of the concentration ratio of calcium to poly(aspartic acid) versus the concentration of used NC-OH dispersion for film preparation (i.e., film thickness) on the mineralization outcome. b) Exemplary SEM images of mineralized films from 0.11 wt% NC-OH dispersion and [Ca^{+2}/pAsp] = 555; c) 1.01 wt% and [Ca^{+2}/pAsp]=555; d) 0.11 wt% and [Ca^{+2}/pAsp]= 11 after one day; e) 0.11 wt% and [Ca^{+2}/pAsp]=11 after three days.

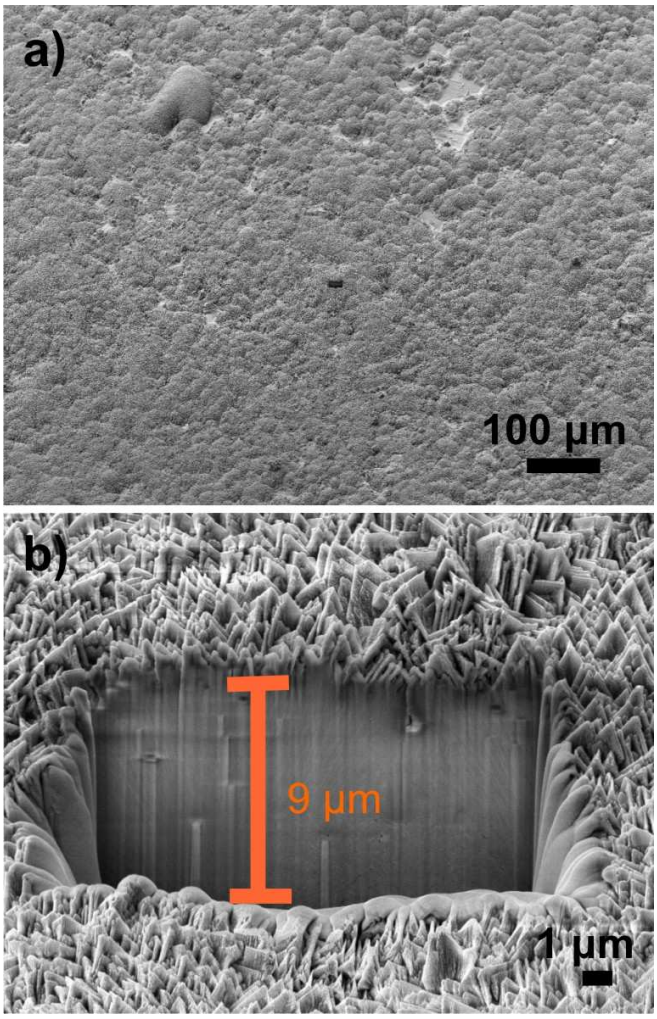

Fig. S9: FIB cut of NC-OH films prepared from a film with a thickness of 750 nm mineralized in the absence of Mg^{+2}. b) shows the morphology of mineralized films in which the platelets of calcite are very well oriented.

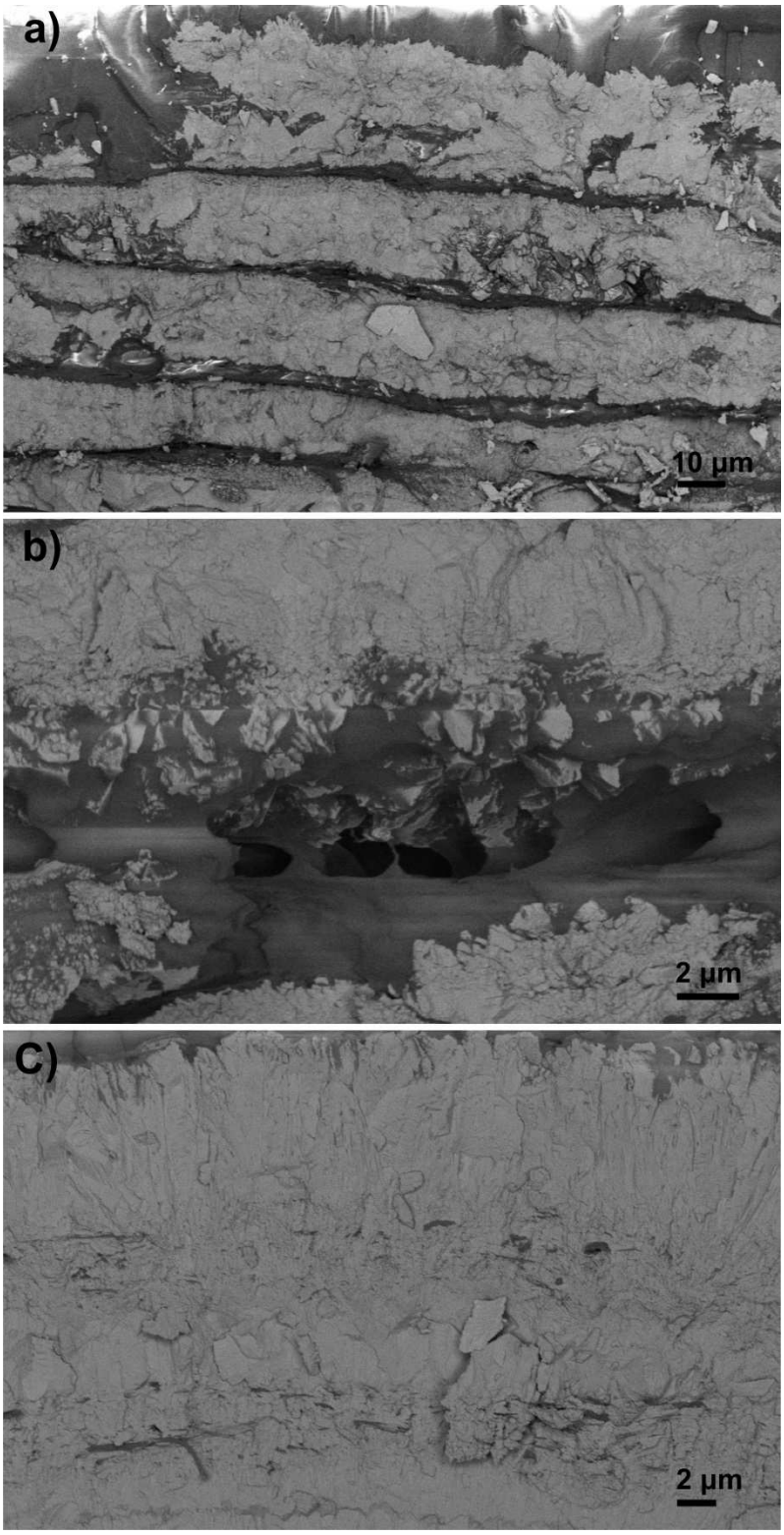

Fig. S10: SEM cross-section view of the film containing layers of NC-OH and NC-COOH after 8 times mineralization (16 layers, 8 layers of mineralized NC-OH and 8 layers of unmineralized NC-COOH). a) Overview. b) Zoom-in on the border between layers. c) Zoom-in on one of the mineralized layers infiltrated into the NC-OH films. Small platelets of calcite crystals can be seen from this section.

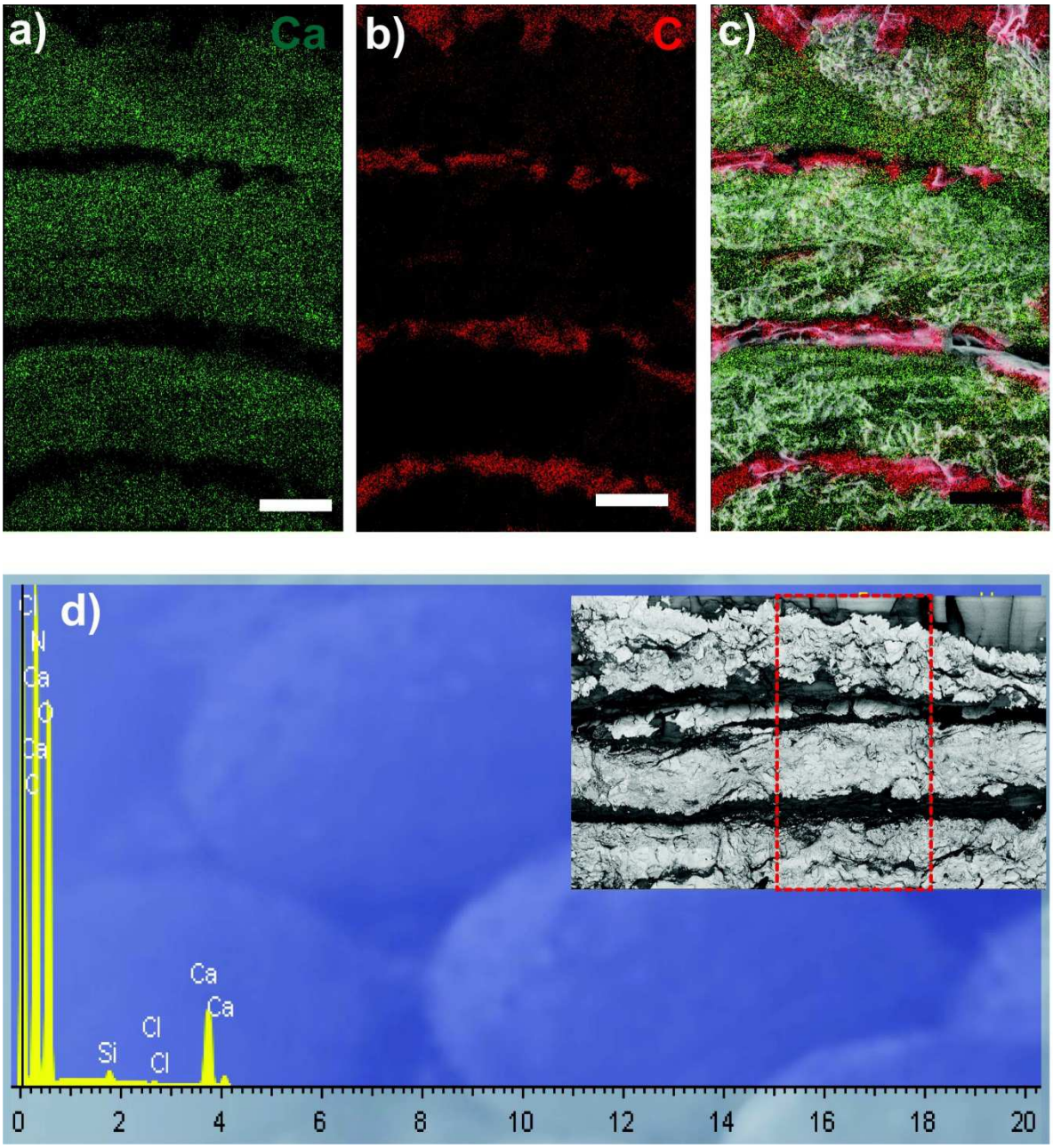

Fig. S11: EDX and elemental mapping of the bio-inspired nacre-like material after 16 mineralizations. a) Mapping of calcium across the sample. b) Mapping of carbon across the sample. c) Overlay of all mappings in combination with secondary electron image of the area in which EDX was taken. d) EDX spectrum of the related mapping. Inset in d shows the electron backscatter SEM image with a marked area from which the spectrum was taken. The scale bars are 10µm.

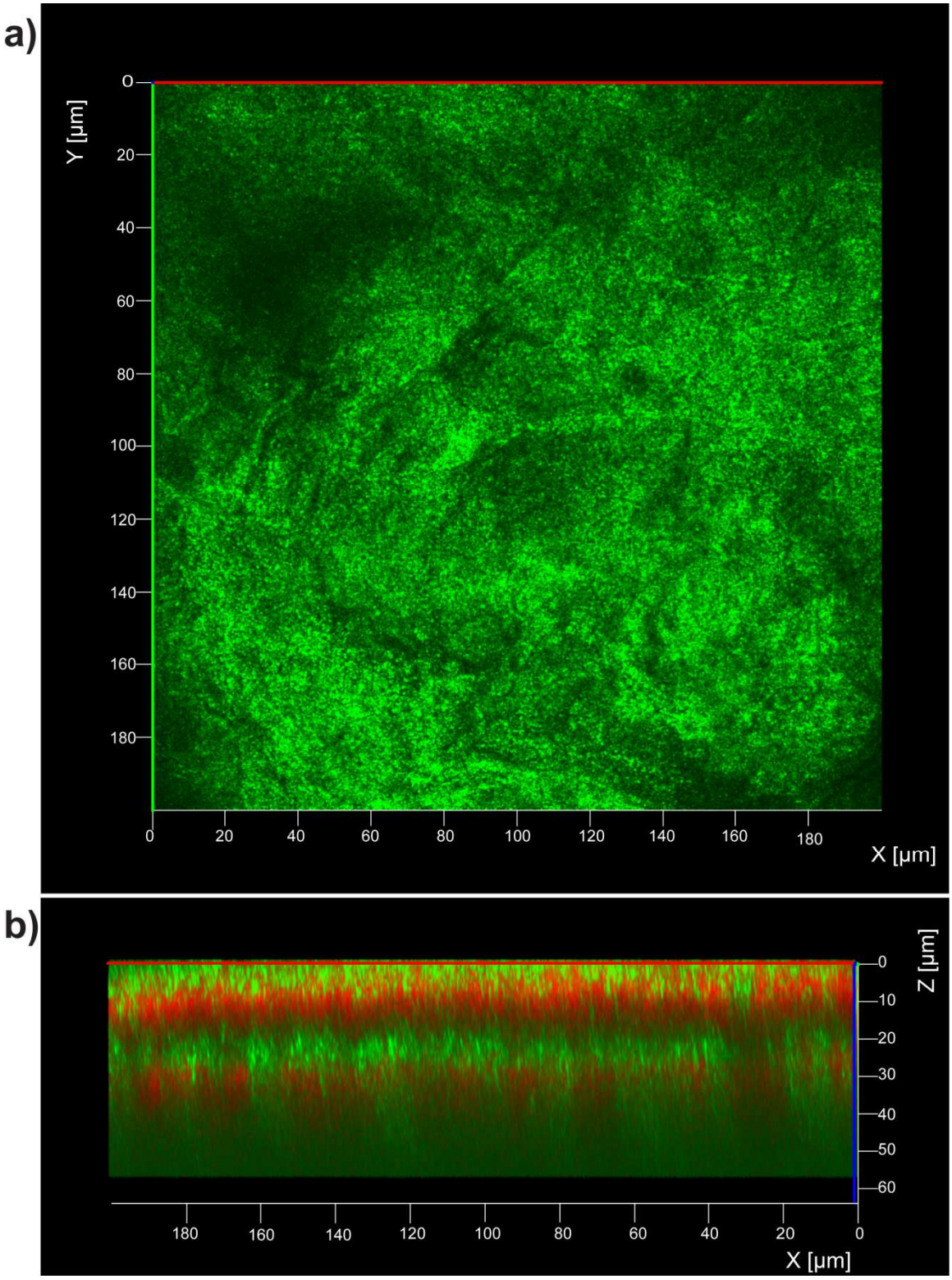

Fig. S12: Confocal microscopy images of a bio-inspired nacre-like material with 25 layers: a) Surface topography of the sample showing the minerals covering the surface. b) A 2D image generated from a 3D reconstruction of a z-stack showing the cross-section of the layered nanocellulose-mineral structure.

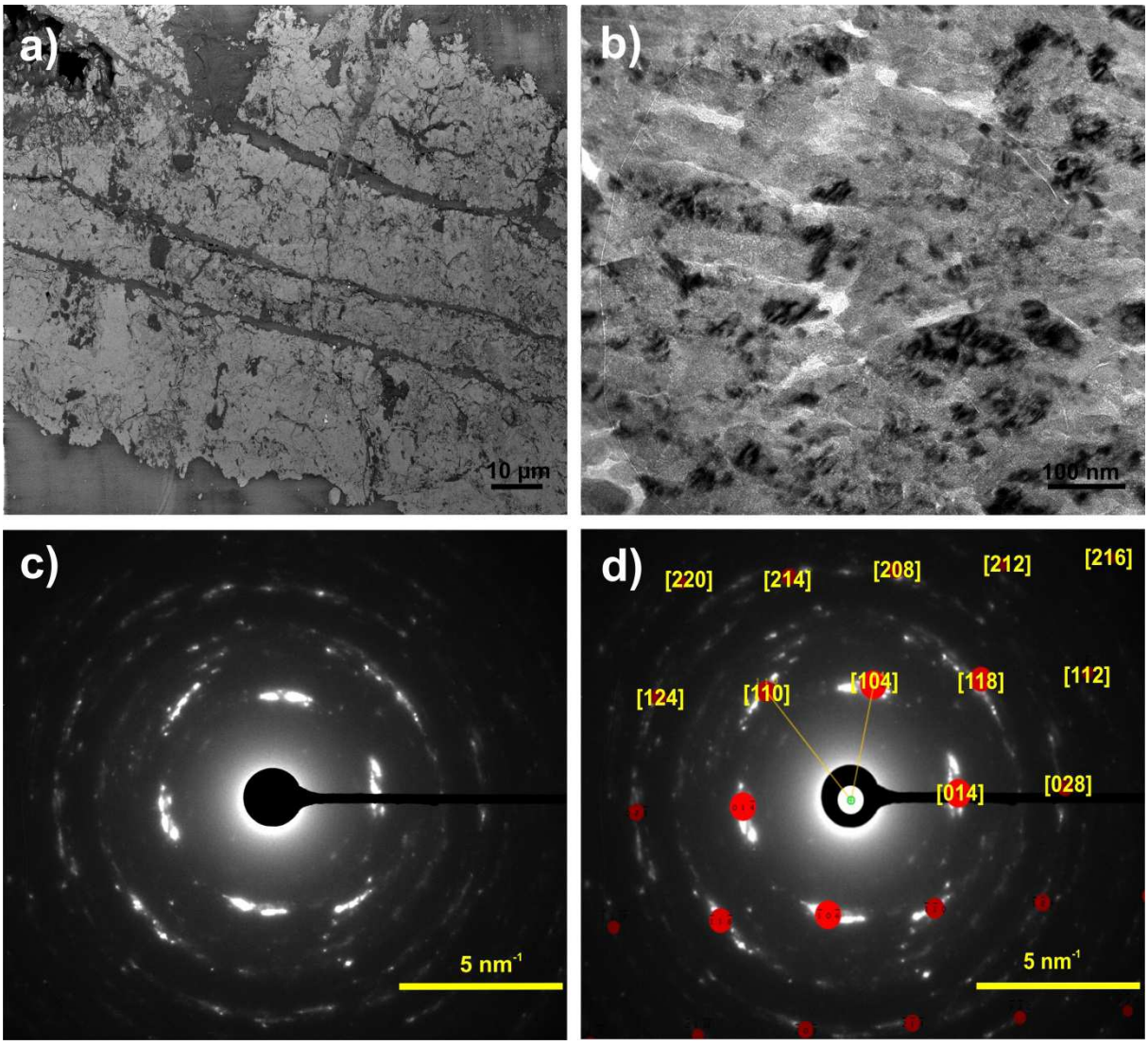

Fig. S13: (a) SEM image of a section of a bio-inspired nacre-like material cut vertically with respect to the film surface. (b) TEM image of the section of a mineralized part. (c) Corresponding SAED of (b). (d) Assignments of reflection spots in SAED, which represent fairly well oriented rhombohedral calcite crystals with a [-441] zone axis.

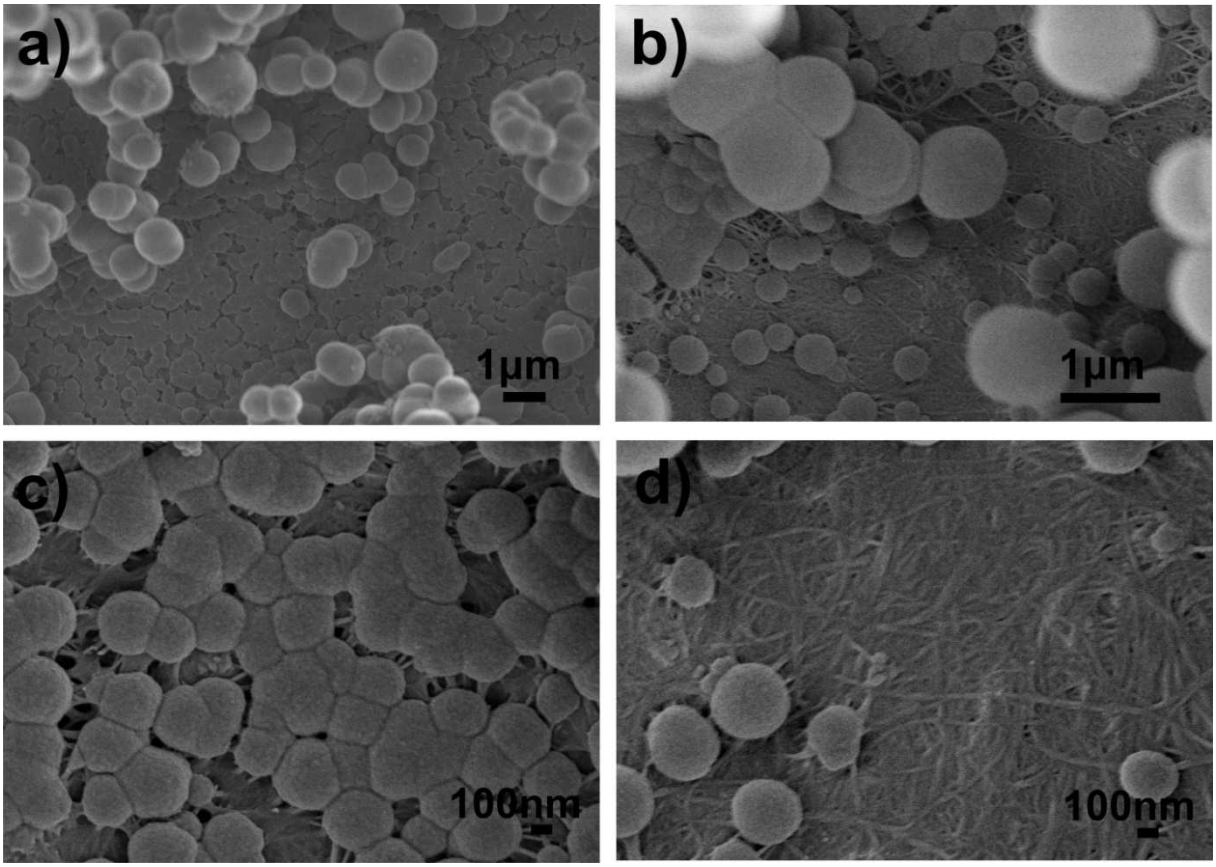

Fig. S14: SEM images of mineralized (a, c) NC-COOH and (b, d) NC-OH films. Mineralization conditions: 5 mM $CaCl_2$, 30 mM Mg^{+2} and 100 µg/ml of poly aspartic acid for 1 day.

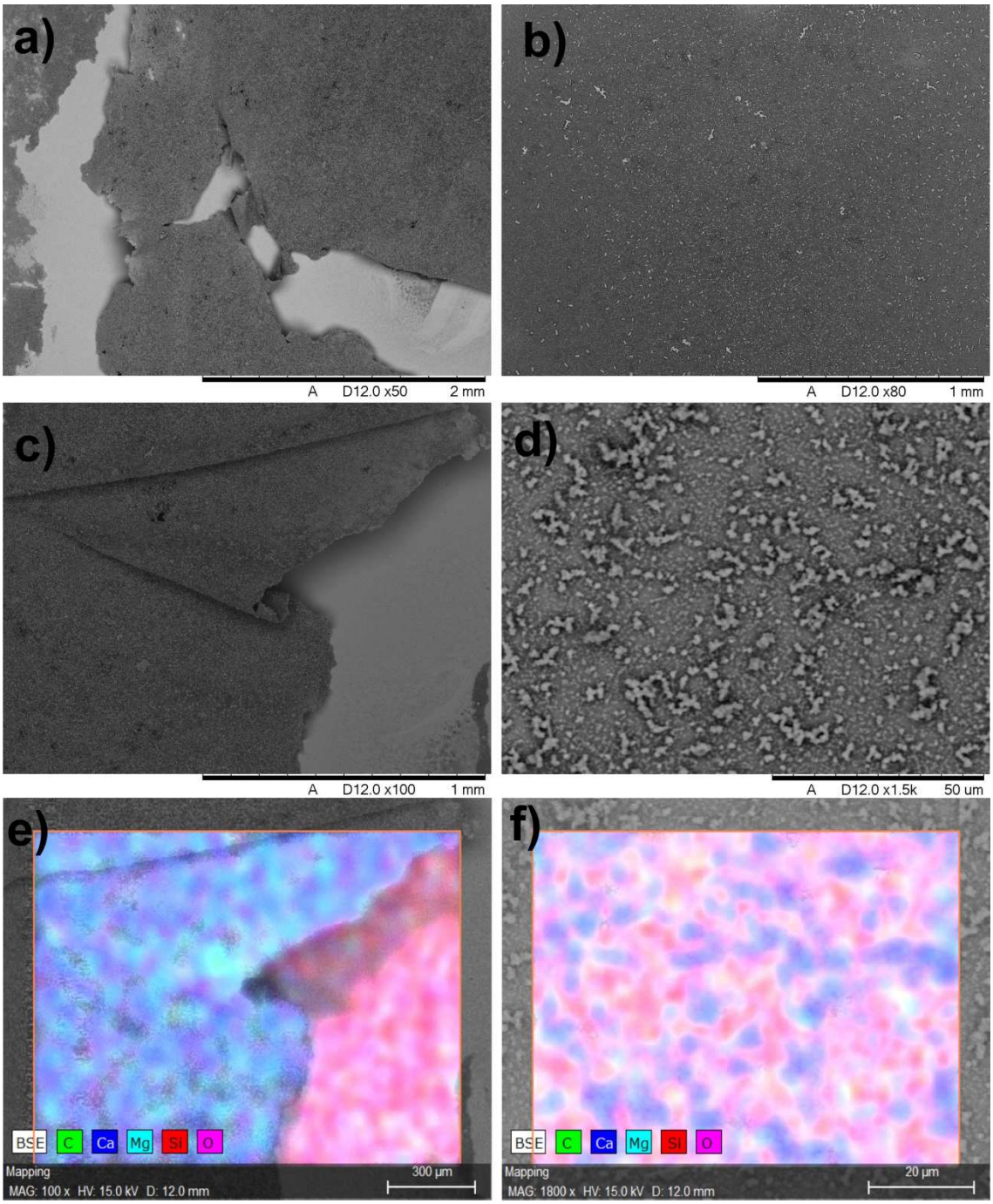

Fig. S15: The SEM images of mineralized layers of NC-OH (a, c) and NC-COOH (b, d) after three days minerlization in presence of 5 mM $CaCO_2$, 30 mM $MgCl_2$ and 100 µg/ml poly aspartic acid. (e) EDX elemental mapping of (c). (f) EDX elemental mapping of (d).

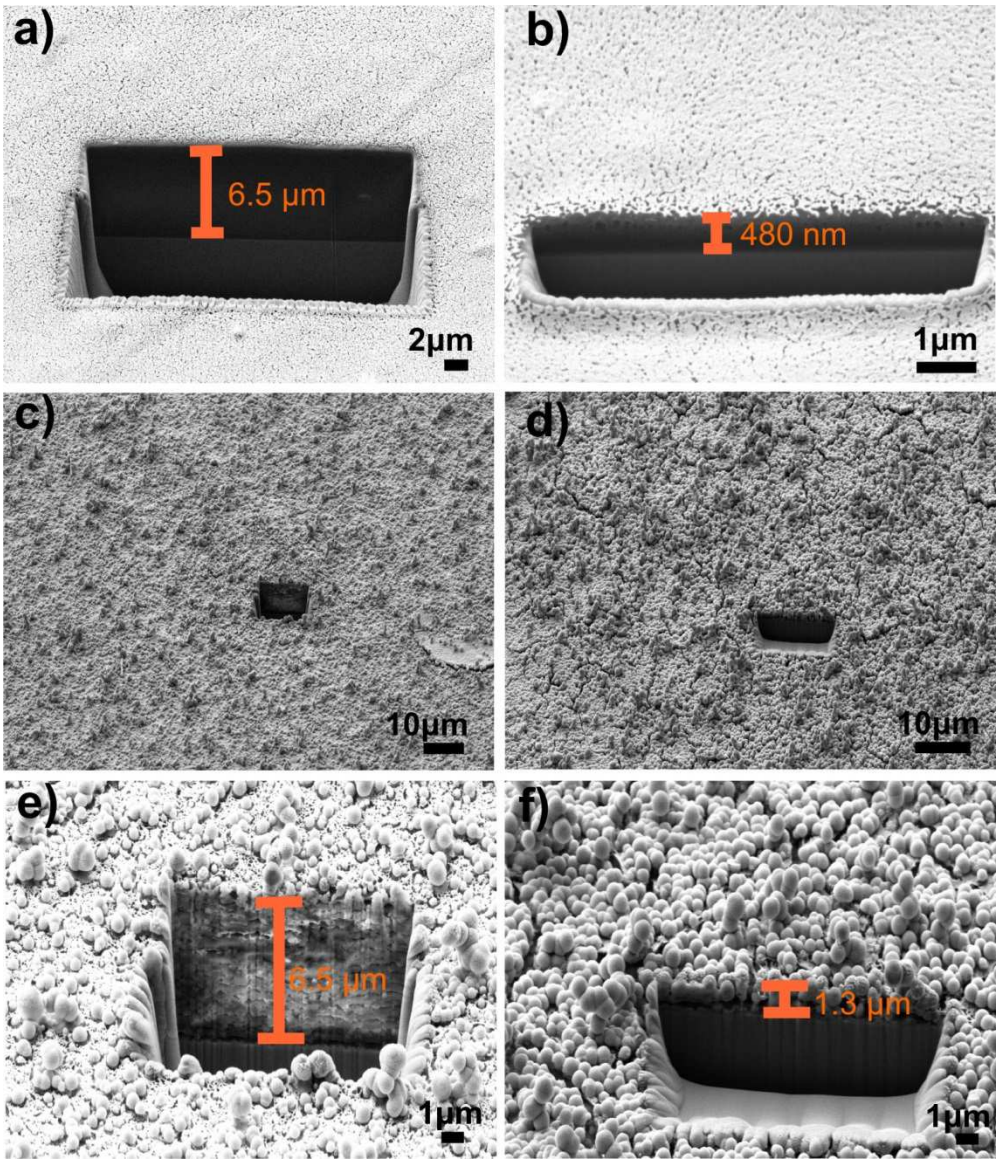

Fig. S16: SEM images of FIB cuts of NC-COOH films prepared from 0.54 wt % dispersions before mineralization (a) and after mineralization (c and e), as well as NC-COOH film prepared from 0.11 wt % dispersions before mineralization (b) and after mineralization (d and f), all in presence of 5 mM $CaCO_2$, 30 mM $MgCl_2$ and 100 µg/ml poly aspartic acid for three days. Images c and d show the overview of mineralized films with FIB cuts showing the complete coverage of ACC particles on the surface.

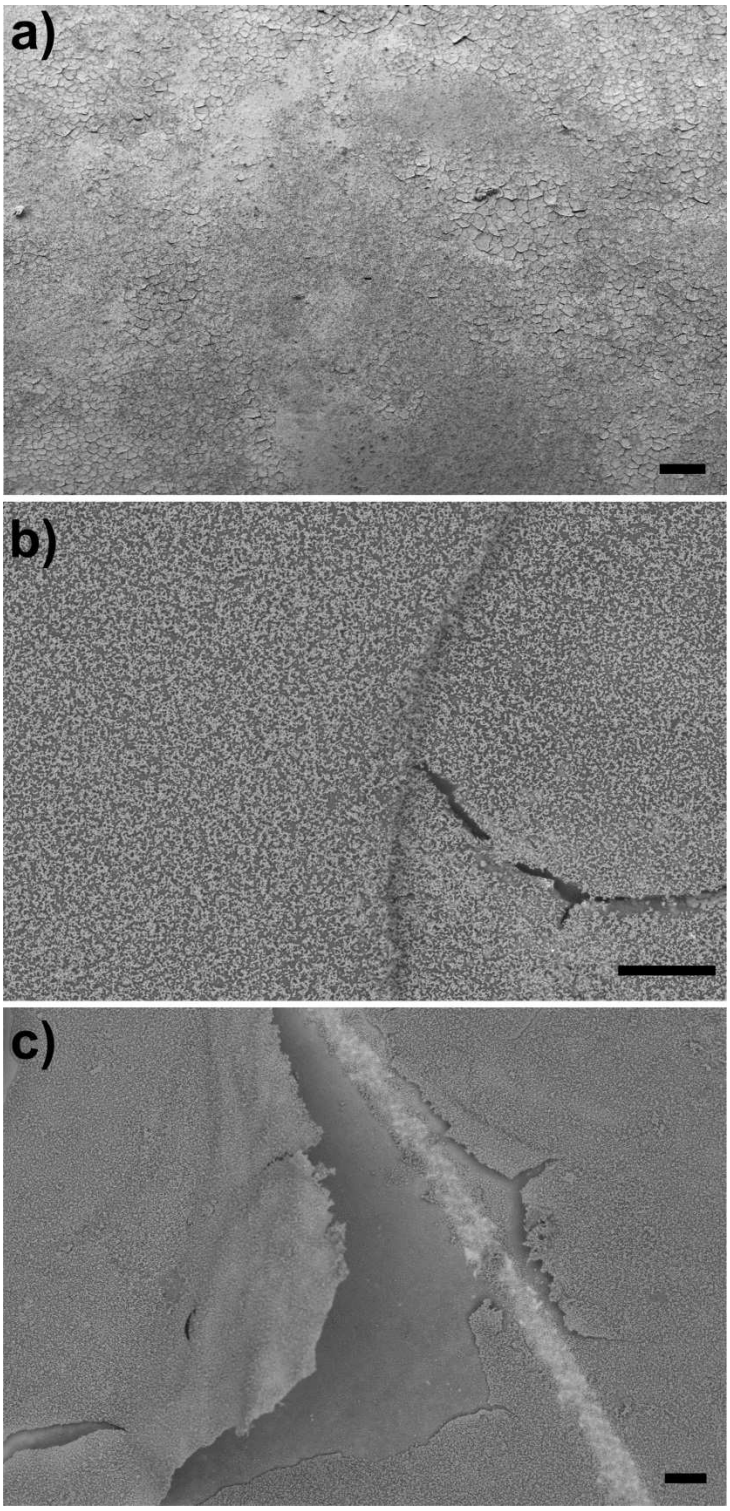

Fig. S17: SEM images of mineralized NC-COOH with layers of unmineralized NC-OH in between, in the presence of Mg^{+2}: a) first. b) second, and c) third mineralization. The fig. shows the development of cracks in the mineralized film, which already exist after the second mineralization (all scale bars 100 µm).

S5 Tables

Table S1: Solution compositions for mineralizations of different nanocellulose films.

Type of Film	Solution content	Solution content
single-layer: NC-COOH	10 mM $CaCl_2$, 50 µg/ml pAsp	5 mM $CaCl_2$, 50 µg/ml pAsp, 30 mM $MgCl_2$
single-layer: NC-OH	10 mM $CaCl_2$, 50 µg/ml pAsp	5 mM $CaCl_2$, 50 µg/ml pAsp, 30 mM $MgCl_2$

Table S2: Mechanical properties obtained from nanoindentation measurements of nacre- like materials with different numbers of layers in comparison with nanoindentation values of *Haliotis laevigata* measured in this work, and values reported for *Haliotis rufescens* in the literature. Also several examples of artificial nacre-like materials have been included from the literature.

sample	Hardness, H (MPa)	Reduced Young's modulus, E_r (GPa)	Plasticity index U_{pl}/U_{tot}	Elastic Recovery U_{el}/U_{tot}	Wear resistance (H/E_r)
90 layers (this work)	222.5 ± 23.6	14.4 ± 1.7	0.836	0.164	0.015
25 layers (this work)	199.5 ± 33.4	9.7 ± 1.5	0.835	0.165	0.020
Haliotis laevigata (this work)	3380 ± 445	67.2 ± 4.8	4.05/7.43 = 0.743	0.256	0.050
Haliotis rufescens[3]	3400 ± 1100	71.24 ± 13.09	N.A.	N.A.	N.A.
Haliotis rufescens[4]	400 (at d_{max} = 150 nm)	30 (at d_{max} = 150 nm)	N.A.	N.A.	N.A.
Nacre-like material based on calcite[8]	97 ± 4.6	4.5	N.A.	N.A.	N.A.
Nacre-like material based on aragonite[9]	1650± 290	43.39 ± 3.21	N.A.	N.A.	N.A.
Polyelectrolyte multilayer infiltrated with $CaCO_3$[10]	6300 ± 300	10.0 ± 0.3	N.A.	N.A.	N.A.

S6 References

[1] M. Henriksson, G. Henriksson, L. A. Berglund, T. Lindstrom, *Eur. Polym. J.* **2007**, *43*, 3434.
[2] M. Salajkova, L. A. Berglund, Q. Zhou, *J. Mater. Chem.* **2012**, *22*, 19798.
[3] J. Y. Sun, M. Z. Ling, Y. M. Wang, D. H. Chen, S. J. Zhang, J. Tong, S. Wang, *J. Bionic. Eng.* **2014**, *11*, 144.
[4] F. Barthelat, C. M. Li, C. Comi, H. D. Espinosa, *J. Mater. Res.* **2006**, *21*, 1977.
[5] J. Y. Sun, B. Bhushan, *RSC Adv.* **2012**, *2*, 7617.
[6] J. K. Berg, T. Jordan, Y. Binder, H. G. Börner, D. Gebauer, *J. Am. Chem. Soc.* **2013**, *135*, 12512.
[7] I. Usov, G. Nystrom, J. Adamcik, S. Handschin, C. Schütz, A. Fall, L. Bergström, R. Mezzenga, *Nat. Commun.* **2015**, *6*.
[8] X. Q. Li, H. C. Zeng, *Adv. Mater.* **2012**, *24*, 6277.
[9] L.-B. Mao, H.-L. Gao, H.-B. Yao, L. Liu, H. Cölfen, G. Liu, S.-M. Chen, S.-K. Li, Y.-X. Yan, Y.-Y. Liu, S.-H. Yu, *Science, DOI:10.1126/science.aaf8991*.
[10] I. F. Patel, M. V. Kiryukhin, N. L. Yakovlev, H. S. Gupta, G. B. Sukhorukov, *J Mater Chem B* **2015**, *3*, 4821.